doi:10.1111/evo.14

Long-term cloud forest response to climate warming revealed by insect speciation history

Antonia Salces-Castellano,[1,2] Sean Stankowski,[3,4] Paula Arribas,[1] Jairo Patiño,[5] Dirk N. Karger,[6] Roger Butlin,[4,7] and Brent C. Emerson[1,8]

[1]*Island Ecology and Evolution Research Group, Institute of Natural Products and Agrobiology (IPNA-CSIC), La Laguna 38206, Spain*

[2]*School of Doctoral and Postgraduate Studies, University of La Laguna, La Laguna 38200, Spain*

[3]*Institute of Science and Technology, Klosterneuburg 3400, Austria*

[4]*Department of Animal and Plant Sciences, University of Sheffield, Sheffield S102TN, United Kingdom*

[5]*Department of Botany, Ecology, and Plant Physiology, University of La Laguna, La Laguna 38071, Spain*

[6]*Department - Dynamic Macroecology, Swiss Federal Research Institute WSL, Birmensdorf 8903, Switzerland*

[7]*Department of Marine Sciences, University of Gothenburg, Gothenburg 40530, Sweden*

[8]*E-mail: bemerson@ipna.csic.es*

Received July 30, 2020
Accepted October 7, 2020

Montane cloud forests are areas of high endemism, and are one of the more vulnerable terrestrial ecosystems to climate change. Thus, understanding how they both contribute to the generation of biodiversity, and will respond to ongoing climate change, are important and related challenges. The widely accepted model for montane cloud forest dynamics involves upslope forcing of their range limits with global climate warming. However, limited climate data provides some support for an alternative model, where range limits are forced downslope with climate warming. Testing between these two models is challenging, due to the inherent limitations of climate and pollen records. We overcome this with an alternative source of historical information, testing between competing model predictions using genomic data and demographic analyses for a species of beetle tightly associated to an oceanic island cloud forest. Results unequivocally support the alternative model: populations that were isolated at higher elevation peaks during the Last Glacial Maximum are now in contact and hybridizing at lower elevations. Our results suggest that genomic data are a rich source of information to further understand how montane cloud forest biodiversity originates, and how it is likely to be impacted by ongoing climate change.

KEY WORDS: **Coleoptera, hybridization, Last Glacial Maximum, Quaternary climate, speciation, trade-wind inversion.**

Cloud forests occur within narrow altitudinal limits and contain highly specialized suites of species dependent on montane topography and cloud-related microclimates (Ponce-Reyes et al. 2012), creating isolated patches of habitat within which thousands of unique species have evolved (Helmer et al. 2019). Although often associated with tropical regions (e.g., Pounds et al. 1999; Still et al. 1999; Foster 2001; Crausbay et al. 2015), they are also a feature of subtropical regions (e.g., Sperling et al. 2004). The montane mesoclimates that give rise to cloud forests are strongly shaped by a temperature inversion associated with large-scale atmospheric circulation patterns, known as the trade-wind inversion (TWI) (Still et al. 1999; Martin et al. 2010). Thus, montane cloud forests are caused by a direct interaction between mountains and the global climate system (Rahbek et al. 2019). Although it has been suggested that such cloud forests may offer stable environments conducive to the long-term persistence of

species (Fjeldså et al. 1999), their dependence upon the global climate system means they are at the same time expected to be dynamic with respect to their distribution limits. Understanding both the direction and magnitude of cloud forest change in response to global climate warming is of fundamental interest, due to the high proportions of endemic species associated with cloud forests, and the ecosystem services that they provide. Montane cloud forests typically harbor an impressive array of plants and animals and high levels of endemicity (Still et al. 1999). In addition, cloud forests act as important local and regional watersheds, which are of particular importance for water provision (Loope and Giambelluca 1998).

Several studies have provided support for a "lifting-cloud-base" (LiftCB) hypothesis (Pounds et al. 1999), whereby atmospheric warming raises the average altitude at the base of the orographic cloud bank. For instance, Still et al. (1999) used a global climate model to predict changes in the elevation of cloud forests for four cloud forest locations, representing four different continents. Based on simulations for the present, the Last Glacial Maximum (LGM), and a CO_2-doubled atmosphere, their results suggest an upslope shift of the cloud layer in response to future warming. Further support for the LiftCB hypothesis comes from Pounds et al. (1999) who analyzed long-term climatic and demographic species data and concluded that declines in anuran populations in Costa Rican cloud forests may be linked to reductions of mist frequency since the mid-1970s. However, more recent analyses raise questions about the generality of the LiftCB hypothesis. Using between 30 and 80 years of daily climate records (for temperature, relative humidity, and the diurnal temperature range), Sperling et al. (2004) infer warmer temperatures to force a downward shift of the lower limits of the orographic cloud formations that sustain laurel forests on the island of Tenerife in the Canary Islands. A similar inference has been arrived at for the Hawaiian Islands. Using downscaling of global warming climate projections in the Hawaii region, Lauer et al. (2013) provide evidence for strong changes of projected climate by the end of the 21st century that include a reduction in the elevation of the TWI. We refer to the model of Sperling et al. (2004) and Lauer et al. (2013) as the "lowering-cloud-base" (LowCB) hypothesis.

Testing between the LiftCB and LowCB hypotheses is of fundamental importance for understanding and potentially managing climate change consequences for montane cloud forest ecosystems, their individual biodiversity legacies (Rahbek et al. 2019), and the ecosystem services they provide (Loope and Giambelluca 1998; Foster 2001). Pollen records can provide an additional data source for evaluating support for either hypothesis (Loope and Giambelluca 1998; Still et al. 1999; Foster 2001; Crausbay et al. 2015), but are reliant on suitable deposition conditions, which are often limited, particularly on oceanic islands. A further potential source of data is the very species that are restricted to, or strongly associated with, montane cloud forests. Species ranges may track changing climate and this may manifest itself in population size changes, fragmentation of ranges, and secondary contact of previously isolated populations (Hewitt 2000; Taylor et al. 2015). Thus, the timing of both speciation and demographic events within species can be used to infer how species have responded to past climate change.

To test explicitly between the LiftCB and LowCB hypotheses, we use genomic data for demographic inference within an invertebrate species tightly associated to the montane cloud forest that characterizes the dorsal ridge of the Anaga peninsula, on the Canary island of Tenerife. Salces-Castellano et al. (2020) have previously sampled 154 species of beetle within this ecosystem to reveal evidence for repeated phylogeographic structuring of mitochondrial DNA (mtDNA) variation within species across a low elevation dorsal saddle, the origin of which dates back to a mega-landslide event estimated to have occurred between 4.1 and 4.7 million years ago. Nuclear genomic analyses for 16 of these species (eight of which present no phylogeographic structure for their mtDNA) revealed phylogeographic structure across the saddle for 13 species, with evidence for admixture in areas close to the saddle for 12 of these species. Divergence estimates within species fell within the Quaternary, and confidence intervals for all but one species did not include the age of the landslide itself. Salces-Castellano et al. (2020) further reveal that landscape patterns of genomic relatedness within species are best explained by environmental and landscape variables related to water stress. They conclude that geographical congruence for both (i) regional structuring within species and (ii) areas of admixture between regions are the result of a dynamic of isolation and secondary contact driven by Quaternary climate oscillations. However, their data do not distinguish between the LiftCB and LowCB hypotheses.

Among the species of beetle studied by Salces-Castellano et al. (2020), *Acalles globulipennis* Wollaston, 1854, presents one of the highest mtDNA divergences between eastern and western populations, suggesting greater power for genome-based model testing, and was the only species sampled in all study sites by Salces-Castellano et al. (2020), suggesting it is likely to be present at intermediate sampling sites. We thus use *A. globulipennis* to increase sampling across its geographical range and perform robust genome-based model testing between the LiftCB and LowCB hypotheses. The LiftCB hypothesis predicts species ranges to be most fragmented during interglacial climate conditions, as lower elevation range limits will be forced upslope by higher water stress (Fig. 1A). In contrast, the LowCB hypothesis predicts water stress to be reduced at lower elevations during interglacial periods, and thus the lower elevation range limits of species will extend downslope, facilitating higher

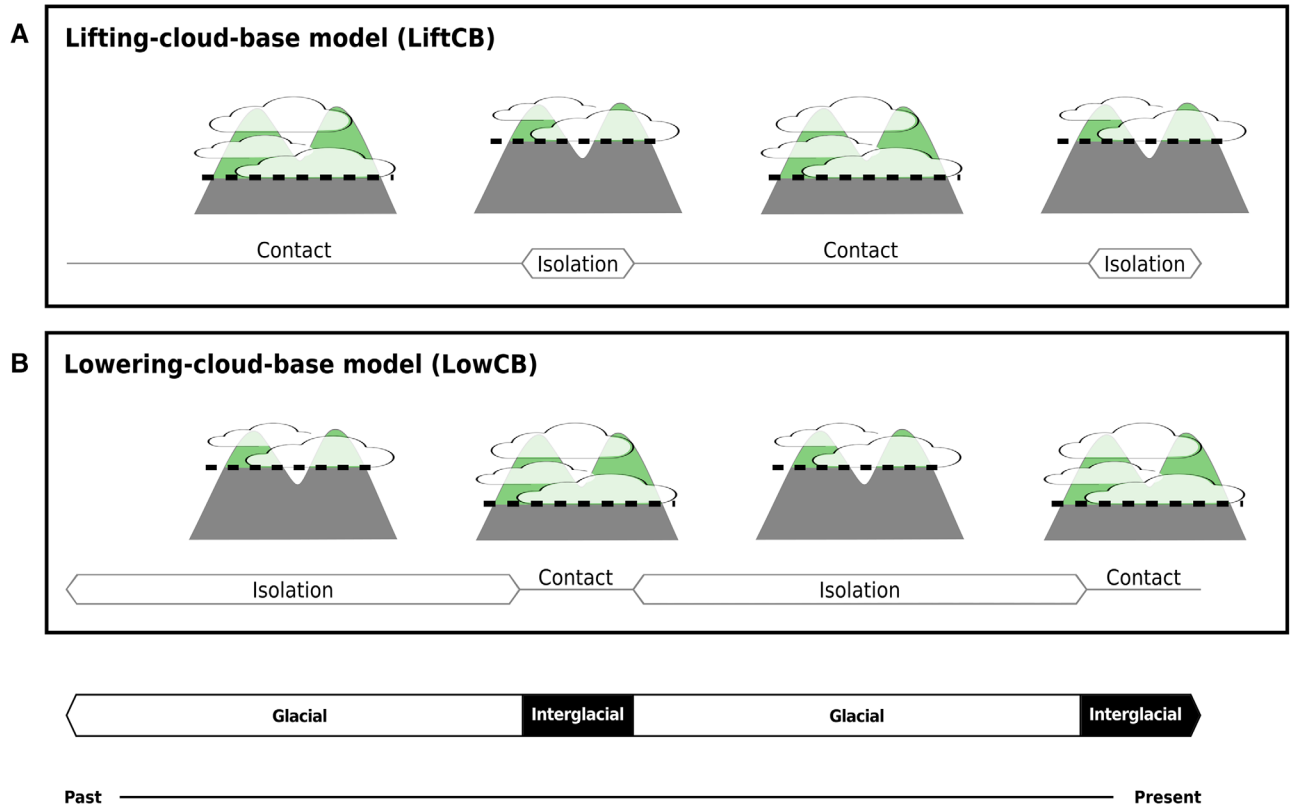

Figure 1. **Competing models of (A) a lifting-cloud-base (LiftCB) and (B) a lowering-cloud-base (LowCB), with reference to predictions for directional changes in the lower elevation limits of orographic cloud formations that sustain montane cloud forests, under a warming climate. In panel A, regional isolation of cloud forest species at higher elevations should be greatest during interglacial periods. In panel B, current interglacial conditions should be characterized by higher population connectivity of cloud forest species at lower elevations.**

connectivity among populations (Fig. 1B). To test between the LiftCB and LowCB hypotheses, we analyze nuclear and mitochondrial variation from 19 populations of *A. globulipennis*, sampled across 14.5 km of cloud forest, focusing sampling around the area of previously described genomic admixture between eastern and western populations (Salces-Castellano et al. 2020). We evaluate the evolutionary origins of admixed individuals to differentiate between (i) an ancient origin, which would be consistent with the LiftCB hypothesis (Fig. 1A), and (ii) an origin due to contemporary gene flow and admixture, which would be consistent with the LowCB hypothesis (Fig. 1B). We also adopt a demographic model-testing framework for explicit comparison between the contrasting expectations of the two hypotheses. We compare models of isolation with and without gene flow and with single or multiple events of contact. Both the LiftCB and LowCB hypotheses predict a cyclical model of isolation with secondary contact, with the LiftCB hypothesis predicting contemporary isolation, whereas the LowCB hypothesis predicts contemporary secondary contact. We additionally compare the temporal duration of isolation and secondary contact. The LiftCB hypothesis predicts that secondary contact will dominate, due to its association with longer duration glacials, whereas isolation is expected to dominate under the LowCB hypothesis.

Material and Methods

SAMPLING

Sampling for *A. globulipennis* was undertaken to augment the 10 sampling sites in Salces-Castellano et al. (2020). Nine new sites were sampled using collection umbrellas and beating forest vegetation to obtain a minimum of five individuals per site. A total of 118 individuals of *A. globulipennis* were sampled from the nine new sites, bringing the total number of individuals available for analysis to 261 across all 19 sites (Fig. 2; Table S1) along the dorsal ridge of the Anaga peninsula. Specimens were placed in 100% ethanol in the field, taxonomically identified in the lab, and then stored at 4°C until DNA extraction.

MtDNA SEQUENCING, ddRAD SEQUENCING, DEMULTIPLEXING, ASSEMBLY, AND FILTERING

All individuals were amplified and sequenced for an approximately 824 bp region of the mtDNA COI. With the objective of generating double-digest restriction site-associated DNA

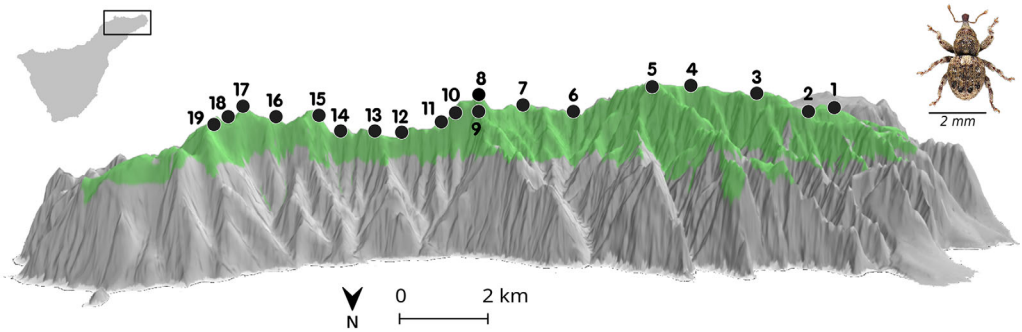

Figure 2. **Sampling sites within the laurel forest of the Anaga peninsula of Tenerife, Canary Islands, labeled from west to east (1–19). The potential extent of the laurel forest within the Anaga peninsula is shown in green (del Arco Aguilar et al. 2006). *Acalles globulipennis* is shown in the top right inset (photo copyright: Peter Stüben).**

sequence (ddRAD-seq) data for five individuals per sampling locality, a total of 64 individuals were selected for ddRAD sequencing (note that in three localities fewer than five individuals were sampled). Full details for mtDNA and ddRAD sequencing can be found in the Supporting Information, together with conditions for ddRAD-seq demultiplexing, assembly and filtering.

PHYLOGENETIC STRUCTURE OF MtDNA VARIATION

To explore patterns of relatedness among mtDNA haplotypes, their phylogenetic relationships were inferred using MrBayes version 3.2.6 (Ronquist et al. 2012). We used the best substitution model obtained from jModelTest version 2.1.7 (Guindon and Gascuel 2003; Darriba et al. 2012) and ran the analysis for 25,000,000 generations, with four simultaneous Markov chains sampling every 10,000 samples, and discarding the first 25% of samples as burn-in.

POPULATION GENOMIC STRUCTURE

Population genomic structure based on the ddRAD-seq data was characterized with a principal component analysis (PCA), including the 95% inertia ellipses for three areas, performed with the R package adegenet version 2.1.1 (Huson and Bryant 2006). East and West areas are defined based on the exclusive presence of single ancestry genotypes, whereas the third contact area is defined by the presence of admixed genotypes. To distinguish single ancestry and admixed genotypes, we first used a cross-entropy criterion to identify the optimal value of K, and then individual admixture coefficients were estimated using Admixture version 1.3.0 (Alexander et al. 2009). Analyses were repeated five times to evaluate consistency of individual ancestry inferences.

HYBRID SIMULATIONS

The LiftCB hypothesis predicts admixed individuals to be of ancient origin, derived from glacial contact, whereas the LowCB hypothesis predicts a recent origin through contemporary gene flow and admixture. To evaluate evidence for these expectations, we investigated admixture between the western and eastern populations using HybridLab (Nielsen et al. 2006). To do this, we used individuals with ≥99.9% eastern or western ancestry to calculate F_{ST} per locus to generate a joint distribution of F_{ST} and minor allele frequency (MAF). Although it has previously been suggested that background selection may contribute to high estimates of F_{ST} (Cruickshank and Hahn 2014), more recently it has been revealed that F_{ST} is largely insensitive to locus-to-locus variation in the intensity of background selection (Matthey-Doret and Whitlock 2019). VCFtools version 0.1.15 (Danecek et al. 2011) was used to calculate F_{ST} per locus and MAF. We then used this distribution to identify a set of loci that are semi-diagnostic (hereafter referred to as SD loci) for eastern and western populations (MAF > 0.4, $F_{ST} > 0.8$). We then used the observed genotypes for SD loci from pure eastern and western individuals (i.e., ≥99.9% eastern or western ancestry) to simulate hybrid individuals using the following crosses: (a) F1; (b) F1 backcross with western parent; (c) F1 backcross with eastern parent; (d) F2; (e) backcross of (b) with western parent; (f) backcross of (c) with eastern parent; (g) backcross of (b) with eastern parent; and (h) backcross of (c) with western parent (Fig. 3A). We generated 100 simulations per cross. For the simulated and observed individuals, we then estimated admixture coefficients with Admixture and plotted these against observed heterozygosity (i.e., proportion of SD loci that were heterozygous). Plots were produced in the "Graphics" package in R version 3.4.4.

DEMOGRAPHIC HISTORY INFERENCE

To estimate population demographic history, we used a modified version (Tine et al. 2014; Rougemont et al. 2017) of the software dadi version 1.7 (Gutenkunst et al. 2009) to analyze the two-dimensional joint site frequency spectrum (2D-JSFS). We compared the fit of 11 models (Fig. 4, *i–xi*) that are variations of four alternative historical scenarios of divergence: strict isolation (SI), and isolation with three different categories of gene flow: continuous migration (IM), ancient migration (AM), and

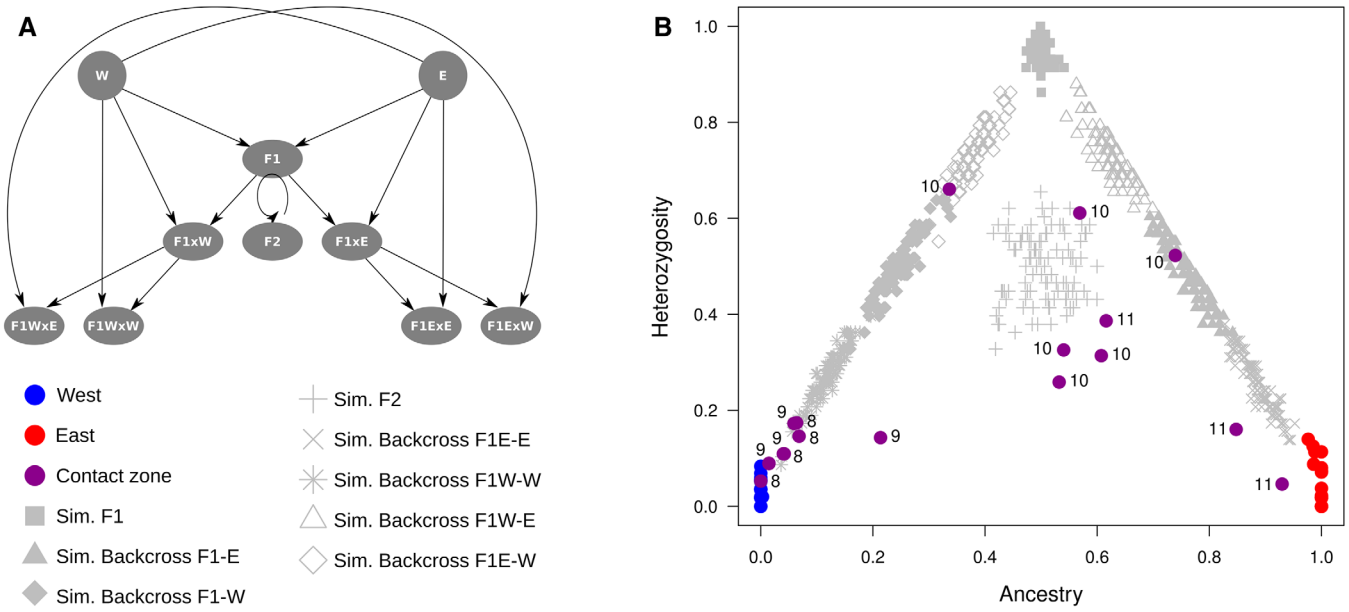

Figure 3. Hybrid simulations for semi-diagnostic (SD) loci from individuals of single ancestry (99.9 %). (A) Summary of the simulated crosses. (B) Simulated and observed genotypes are plotted to represent ancestry and heterozygosity, distinguishing among western (blue), eastern (red), and the contact zone (purple).

secondary contact (SC). Under strict isolation (*i*: SI), an ancestral population splits into two daughter populations that diverge for Ts generations without subsequent gene flow. Under isolation with migration (*ii*: IM), the divergence of the daughter populations is followed by T_S generations with continuous gene flow. Under ancient migration (*iii*: AM), gene flow occurs early in divergence, lasting T_{AM} generations, but then ceases for the remaining T_S generations up until the present. Under secondary contact (*iv*: SC), the split is followed by a period of allopatry lasting T_S generations and then by gene flow for T_{SC} generations at rates m_{12} (east to west) and m_{21} (west to east) from when the populations re-contact up to the present. We also fitted models with multiple periods of isolation and gene flow, which more closely fit expectations for sequential glacial cycles. This was achieved by modifying the AM and SC models to incorporate two different periods of ancient migration (*v*: PAM) and secondary contact (*vi*: PSC). To evaluate potential limitations to gene flow across the hybrid zone due to local adaptation or reproductive isolation, models that included gene flow (*ii*–*vi*) were extended (2M; models *vii*–*xi*) to account for heterogeneous migration across the genome by considering two categories of loci (with proportions P and 1 – P), the first one containing loci that behave neutrally with "unrestricted" gene flow and the second comprising loci with "restricted gene flow" that experience reduced effective migration rates. For each of the two categories, migration rate is estimated for both directions, and we present values for total or unrestricted migration (m_{12} and m_{21}), and migration for restricted loci (m_{e12} and m_{e21}). The 11 models were fitted independently using a hot and a cold simulated annealing procedure followed by Broyden–Fletcher–Goldfarb–Shanno (BFGS) optimization. Ten independent runs were performed for each model, and the run providing the lowest AIC was retained for comparisons among models. A conservative threshold was applied to retain models with $\Delta AIC_i = AIC_i - AIC_{min} \leq 10$, because the level of empirical support for a given model with a $\Delta AIC_i > 10$ is essentially zero (Burnham and Anderson 2002).

The observed 2D-JSFS was constructed using the ddRAD-seq dataset with no MAF filter. We excluded individuals of mixed ancestry to avoid potential confounding effects of contemporary hybridization on the inference of long-term gene flow (Rougemont et al. 2017). A folded JSFS was used, due to the absence of an outgroup. To account for missing data and to maximize the number of segregating sites used in analyses, both populations (East and West) were projected down to smaller sample sizes (20 individuals per population) as recommended in the dadi manual.

To convert the parameters into biologically meaningful values, we used the value of theta (θ) estimated for each model to calculate the ancestral population size using the formula: $N_{ref} = \theta/4L\mu$, where L is the proportion of sites included in the analysis from the total number of sites possible and is calculated as $L = zy75/x$, where z is the number of SNPs included in the analysis, and x is the number of SNPs originally called from y RADtags of 75 bp (Rougeux et al. 2017). In the absence of a mutation rate for Coleoptera, we calculated the value of N_{ref} using the estimated mutation rate for *Drosophila* of 2.8×10^{-9}

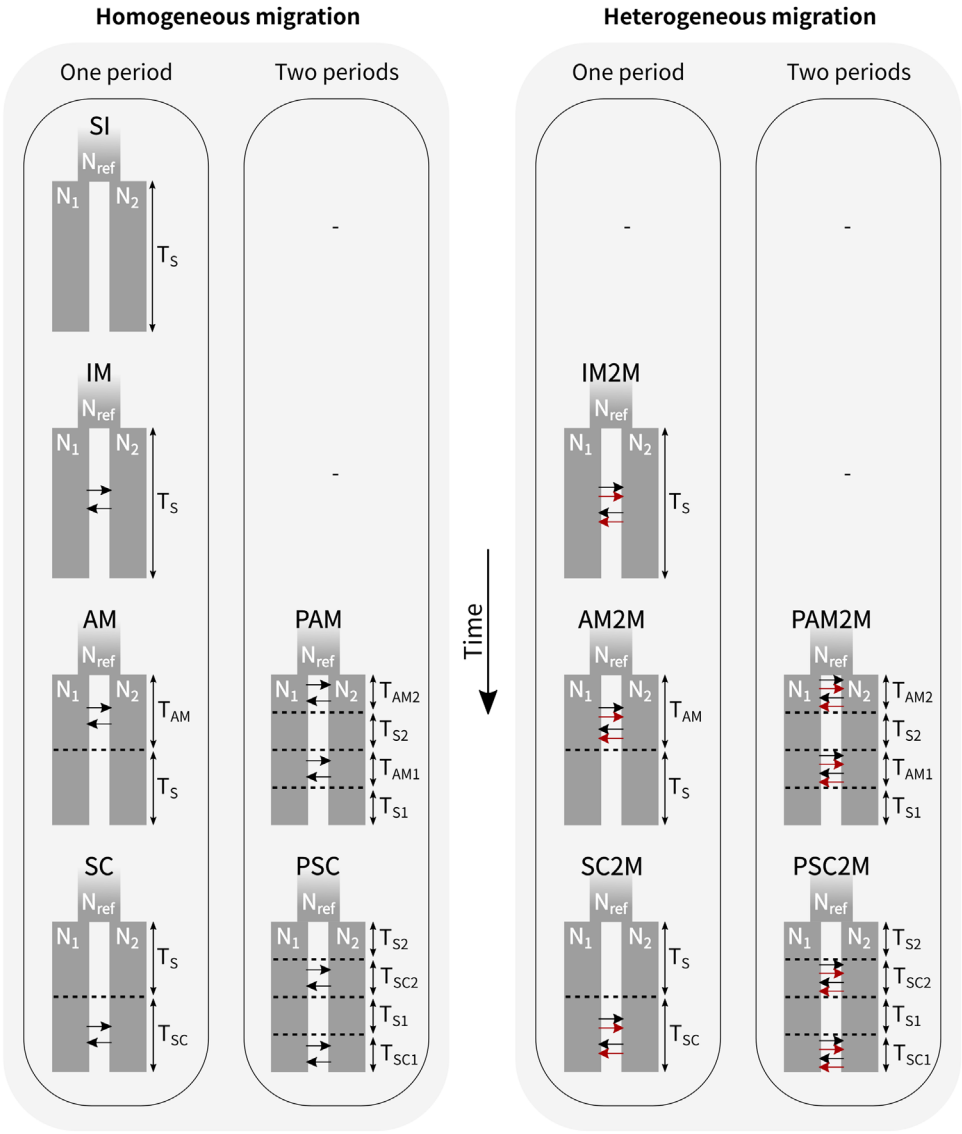

Figure 4. Demographic models for *Acalles globulipennis* representing four alternative modes of divergence: strict isolation (SI), and isolation with three different categories of gene flow: migration (IM), ancient migration (AM), and secondary contact (SC). Each model consists of an ancestral population of size N_{ref} that splits into two populations of effective size N_1 (West) and N_2 (East) during T_S (for models with SI and IM divergence models), $T_{AM} + T_S$ (for models taking into account AM), or $T_S + T_{SC}$ (for models considering SC) generations, possibly exchanging migrants (black arrows) during T_S (for IM models), T_{AM} (for AM models), or T_{SC} (for SC models) generations at rate m_{12} from eastern to western population, and m_{21} in the opposite direction. Models with two different periods of AM or SC are labeled with P (PAM, PSC, PAM2M, and PSC2M). Models of divergence with gene flow extended to account for heterogeneous migration across the genome by considering two categories of loci ("unrestricted (neutral)" and "restricted" gene flow) are labeled with 2M (IM2M, AM2M, SC2M, PAM2M, and PSC2M). Reduced effective migrate rates ($m_{(e)12}$ and $m_{(e)21}$) are represented with red arrows.

substitutions/site/generation (Keightley et al. 2014). A marginally faster rate estimate of 2.9×10^{-9} for *Heliconius melpomene* (Keightley et al. 2015) suggests some degree of generality of this rate across holometabolous insects. Estimated western and eastern population sizes were multiplied by N_{ref} to calculate the size in individuals, and estimated migration rates were divided by $2N_{ref}$ to calculate the proportion of migrants in a population per generation. The number of migrants per generation was calculated by multiplying the proportion of migrants per generation by the population size. Finally, times were converted into generations by multiplying by $2N_{ref}$, considering a generation time of 1 year. To obtain the 95% confidence intervals, we applied a pipeline (https://github.com/QuentinRougemont/DemographicInference) to carry out uncertainty analysis using Godambe Information Matrix methods (Coffman et al. 2016) with 100 bootstrap

replicates. Uncertainty estimates were converted into demographic units by applying uncertainty propagation techniques.

GEOGRAPHICAL CLINE ANALYSES

We used one-dimensional cline analyses to estimate the location of the contact zone and quantify the geographic scale of introgression between eastern and western gene pools, exploring spatial variation in the following measures: mtDNA ancestry, nuclear admixture coefficients, hybrid indices, and allele frequencies for SD loci. To represent mtDNA ancestry, we used the Bayesian tree described above to estimate the proportion of individuals from each of the two principal mtDNA clades described by Salces-Castellano et al. (2020). We used individual nuclear admixture coefficients described above to calculate the average admixture coefficient for each site. Hybrid indices and allele frequencies were estimated using the subset of SD loci (see above). Hybrid index scores (the proportion of western alleles at SD loci) for all the individuals were calculated using a custom R script (van Riemsdijk et al. 2019) and the frequency of western alleles from read counts was obtained with vcftools version 0.1.15 (Danecek et al. 2011) and an R script modified from Westram et al. (2018).

Geographical distances among sampling localities were calculated in QGIS version 3.2.3, to obtain a linear transect to which clines were fitted using a classic equilibrium cline model. This model is based on a sigmoid change of each measure across the contact zone, described by four parameters: the minimum and maximum values in the tails of the cline (Pmin and Pmax), the geographic position of the cline center (c), and the cline width (w), defined as the ratio between the change in allele frequency or trait value of the tails (Pmax – Pmin) and the maximum slope (Barton and Gale 1993). For fitting clines, we used maximum likelihood estimation (function mle2 from the bbmle package: Bolker 2017), implemented in a R script modified from Westram et al. (2018). Cline parameters were then used to plot the clines using the "Graphics" and "Smisc" (Sego 2016) packages in R version 3.4.4.

Results

MtDNA SEQUENCING AND PHYLOGENETIC ANALYSIS

MtDNA sequences were already available for 88 of the 261 individuals (Salces-Castellano et al. 2020). MtDNA sequencing of the remaining 173 individuals resulted in a 96% success rate, yielding a total of 257 sequences. Sequences from four individuals from sites 8 (1) and 10 (3) presented double peaks, almost all at informative sites distinguishing the eastern and western clades. This is most plausibly explained by co-amplification and sequencing of mtDNA of one clade with one or more nuclear mtDNA copies of the other clade, a phenomenon associated with hybridization (Miraldo et al. 2012). The Bayesian phylogenetic tree (Fig. S1) assigned all haplotypes to the two monophyletic clades previously inferred by Salces-Castellano et al. (2020). However, an individual from site 9, which is mainly represented in the West, was found in the eastern clade, and vice versa for an individual from site 10.

DEMULTIPLEXING, ASSEMBLY, AND FILTERING OF ddRAD-seq DATA

A total of 14 individuals were removed due to a low number of reads (1) or more than 30% missing data (13), reducing the dataset from 64 to 50 individuals. These were demultiplexed, assembled, and filtered together with 22 additional individuals from Salces-Castellano et al. (2020), for a total of 72 genotyped individuals. A total of 108,175,096 raw reads were sequenced across all 72 individuals, of which 107,725,931 passed the quality filtering steps of ipyrad (Eaton and Overcast 2020), yielding an average of 1,496,193 raw reads per individual, which reduced to 3,267,362 total reads and 45,380 reads per sample after filtering. The final matrix comprised 14,387 biallelic SNPs across 1999 loci, with 10.31% of missing data, a mean coverage of 27× across all loci and individuals, and a SNP calling error rate (Mastretta-Yanes et al. 2015) of 0.007.

POPULATION GENOMIC STRUCTURE

Both PCA and Admixture analyses provided consistent results supporting individuals from sites 1–7 and from sites 12–19 as single ancestry western and eastern genotypes, respectively, whereas individuals from central sites (8–11) are consistent with a history of admixture. The first component of the PCA clearly describes separation between western and eastern individuals (Fig. 5A). Individuals from sites 8 to 11 spanned the first component, with spatial patterns of relatedness broadly correlating with geography, with individuals from site 10 showing scores around 0. In Admixture analyses, $K = 2$ was optimal, and a transition from western to eastern genotypes was well defined for the ancestry proportions for ddRAD-seq data (Figs. 5B and 5C; Table S2). Samples from sites 8–11 showed mixed ancestry between western and eastern populations, with an approximately equal mix in site 10.

HYBRID SIMULATIONS

The joint distribution of F_{ST} and MAF (Fig. S2) revealed a group of 58 highly differentiated loci for MAF values higher than 0.4, with F_{ST} values between eastern and western populations higher than 0.8. Simulations with HybridLab using the 58 SD loci provided strong diagnosability for a recent hybrid origin for multiple individuals from sites 8 to 11 (Fig. 3B). Several individuals had genotypes consistent with them having second- (F2, and F1 backcross with East) and third-generation parental ancestry

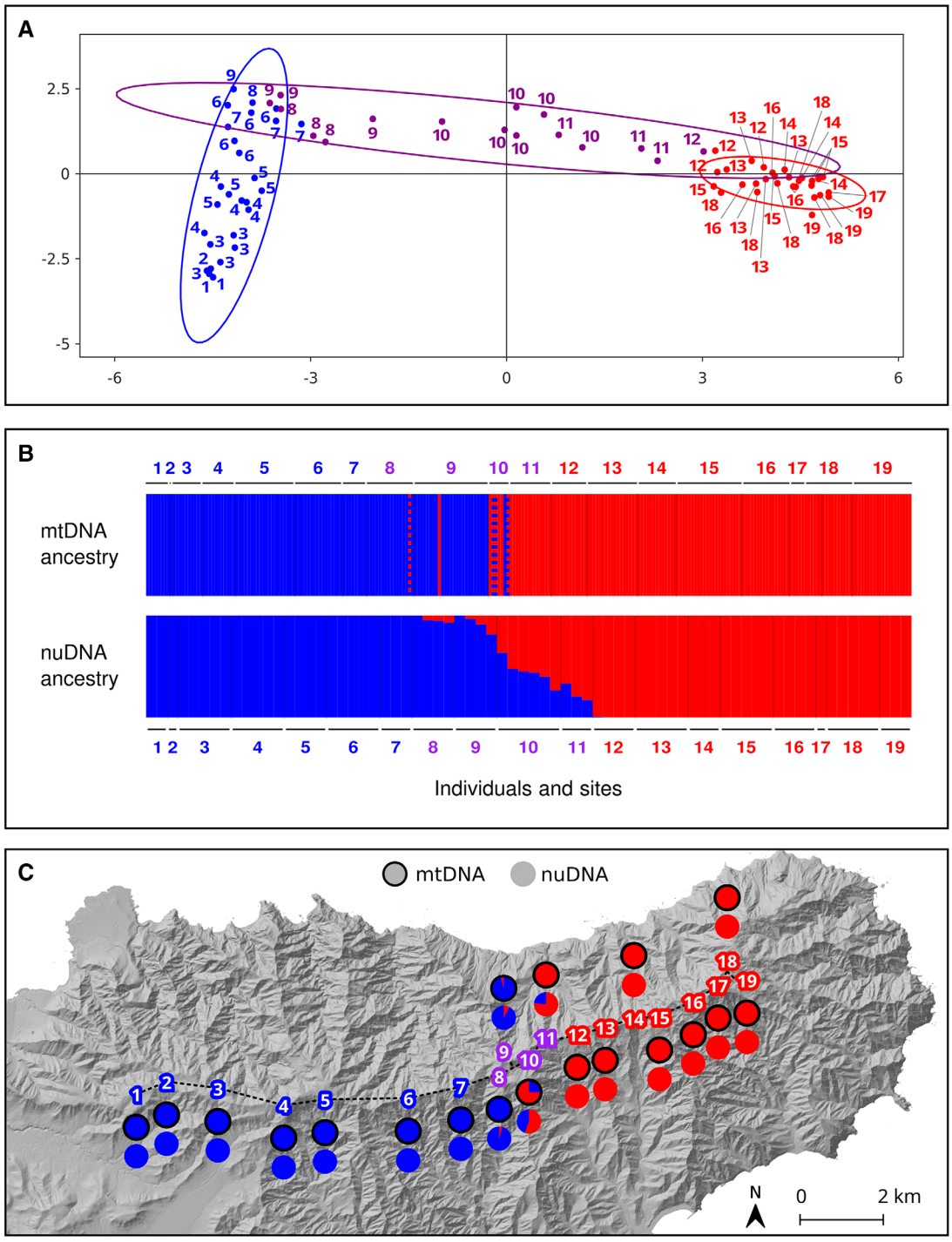

Figure 5. Population genomic structure in *Acalles globulipennis* across the Anaga peninsula of Tenerife. (A) Principal component analysis (PCA) based on the ddRAD-seq data, including the 95% inertia ellipses for three populations: West (blue), contact zone (purple), and East (red). Individuals are colored according to their ancestry proportions corresponding to each population. Sampling site is shown for each individual. (B) Individual ancestry coefficients corresponding to West (blue) and East (red) are shown across the sampling sites for nuclear ddRAD-seq (nuDNA) and mitochondrial (mtDNA) data. Individuals presenting double peaks for mtDNA sequences are represented by a blue and red dashed line. (C) Means of individual ancestry coefficients for each sampling site are spatially represented across the Anaga peninsula. MtDNA ancestry is defined by assignment of individuals to either the West and East clades identified by Salces-Castellano et al. (2020). Individuals with double peaks are not presented. Sampling sites with individuals of mixed ancestry are colored in purple.

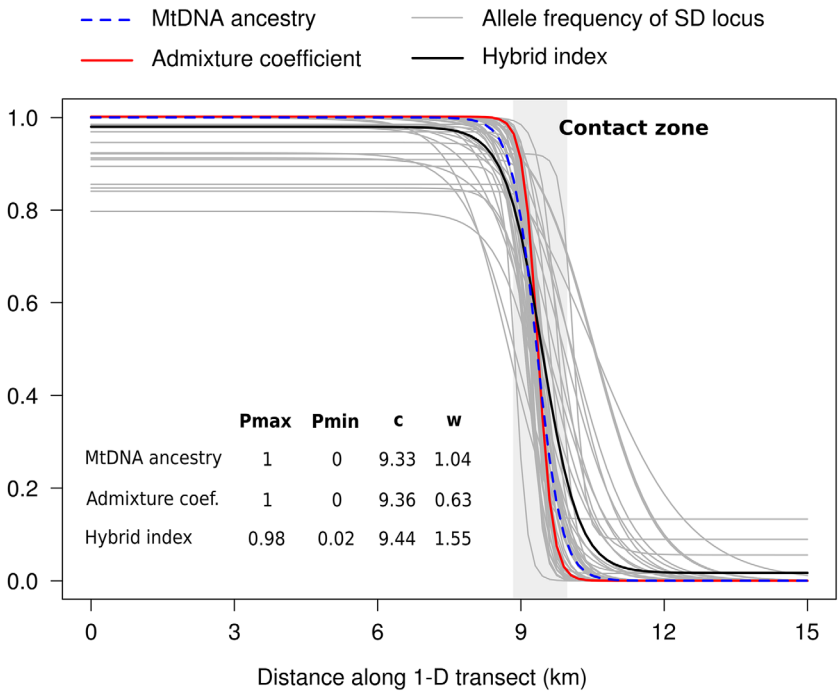

Figure 6. **Geographical clines with respect to the frequencies of west values of mitochondrial DNA (mtDNA) ancestry, admixture coefficient, hybrid index, and allele frequencies of SD loci, across a one-dimensional (1-D) transect from 0 (West) to 15 (East) km. The contact zone is indicated in gray. Cline parameters for each measure are presented: Pmax=the maximum observed value for a measure corresponding the western limit of the cline, Pmin=the minimum observed value for a measure corresponding the western limit of the cline, c=center, and w=width.**

(F1-East backcross with West, and F1-West backcross with West). F1 were not observed, but they must be viable and fertile. Not all individuals were consistent with being recently formed hybrids, suggesting they are later-generation intercrosses or backcrosses, typical of a well-mixed hybrid zone.

DEMOGRAPHIC HISTORY INFERENCE

Model comparison revealed that models including historical gene flow were a much better fit than a model of strict isolation (ΔAIC $>$ 270; Table S3; Fig. S3). The best fitting model included two periods of secondary contact with heterogeneous migration rates (PSC2M). A similar but simpler model involving only one period of secondary contact (SC2M) also provided a good fit to the data with a ΔAIC of 4.3, whereas all other models involved ΔAICs higher than 50. For both the PSC2M and SC2M models, the ratio of secondary contact to divergence time (*T*sc/*T*s) indicated a relatively short duration of introgression with values of 5% and 3.5% of the time since separation, respectively. The proportion of loci estimated to be flowing freely between both populations was 0.5 for both models, indicating that about 50% of loci are subject to a reduced effective migration rate between the two populations. Population size estimates (Table S3) ranged from approximately 991,000 individuals (West) to 778,000 individuals (East) for the best fit model, with very similar values for the second-best fit model (around 951,000 West, and 829,000 East). Estimated time since the initial divergence between eastern and western populations was 1.64 million years ago for the PSC2M model and 1.55 million years ago for the SC2M model. The best fit model showed a migration rate for the "unrestricted" class of loci of approximately six individuals per generation in both directions, whereas the second-best fit model achieved a slightly higher difference between directions, with around seven individuals per generation from East to West and nearly four from West to East. The effective migration rate for the "restricted gene flow" loci from East to West was 0.1 for both of the models, whereas it ranged from 0.08 for the PSC2M model to 0.06 for the PSC2M model when the migration direction was from West to East.

GEOGRAPHICAL CLINE ANALYSES

Clines are presented with respect to the frequencies of the West allele or genome proportion for each measure. Clinal analyses of mtDNA ancestry, nuclear admixture coefficients, hybrid indices, and allele frequencies all revealed a clear and spatially restricted transition from West to East (Fig. 6), with mean values in the ends of the cline ranging from 0.99 (mean Pmax) in the west to 0.01 (mean Pmin) in the east. The average of all cline centers was 9.40 $\pm$ 0.06 km from the most western site, approximately 70 m to the east of site 10 (Table S4), and the average width was

1.11 ± 0.39 km. Independent allele frequency clines for the 58 SD loci showed a very similar shape to the other three measures, with cline centers ranging from 8.75 to 10.55 km, and widths ranging from 0.5 to 4 km. The cline end values ranged from 0.98 (mean Pmax) to 0.01 (mean Pmin), although this range was lower for a few loci that achieved Pmax about 0.8 and a single locus showing Pmin of 0.13 (see Table S4 for detailed results). These results demonstrate the existence of a hybrid zone between East and West, which coincides with central sampling sites 8–11.

Discussion

Genomic data for *A. globulipennis* provide multiple lines of supporting evidence for the lowering cloud base (LowCB) hypothesis (Fig. 1), where atmospheric warming is predicted to lower the average altitude of the base of the orographic cloud banks that sustain cloud forests (Sperling et al. 2004). Sampling reveals that the lower elevation range limit of *A. globulipennis* extends down to at least the lowest elevations of the dorsal ridge of Anaga, indicative of a continuous contemporary distribution. Direct support for the LowCB hypothesis is provided by the hybrid simulations and PCAs that reveal that East and West populations are currently in contact and hybridizing. Clinal analyses reveal the center of the hybrid zone to be approximately 70 m to the east of sampling site 10, approximately 1.3 km west of the low elevation area of the dorsal ridge, identified by Salces-Castellano et al. (2020) as the area of highest water stress across the dorsal ridge. This is consistent with post-LGM range expansion of the eastern population across the low elevation region and secondary contact with the western population.

Demographic inference also provides support for the LowCB hypothesis. Demographic analyses for *A. globulipennis* favored models involving isolation and secondary contact over models of strict isolation, isolation with gene flow, or isolation with initial gene flow followed by strict isolation. Irrespective of whether gene flow was modeled as homogeneous or heterogeneous, the two models incorporating isolation and secondary contact provided a much better fit to the data than alternative models. Although the difference was only marginal, in both cases a model involving multiple events of isolation and secondary contact provided the better fit of the two best models. Converting estimates to real time yielded a time since initial East-West divergence within *A. globulipennis* of 1.6 million years ago (±0.26) and 1.5 million years ago (±0.22) for the best fit and second-best fit models, respectively (Table S3). These estimates fall below the higher posterior density (HPD) derived from mtDNA estimates (4.6 [HPD: 2.5–7.0]). Although both mtDNA and nuclear DNA estimates are subject to error due to uncertainty surrounding the appropriateness of the external rates used, both imply origins for divergence deep into the Quaternary or beyond. These divergence time estimates, together with the best-supported demographic model, are best explained by a history of repeated isolation and secondary contact for *A. globulipennis*, mediated by cyclical transitions between glacial and interglacial climate.

Further demographic support for the LowCB hypothesis is provided by the estimated durations for periods of isolation and secondary contact. The globally best fit model of repeated isolation and secondary contact with heterogeneous gene flow infers relatively brief intervals of secondary contact (approximately 5% of total time), implying long intervals of population isolation. The next best fit model of a single event of isolation and secondary contact yielded a similar inference, with only 3.5% of time estimated to involve secondary contact. These time estimates are consistent with the LowCB hypothesis, where long periods of isolation at higher altitudes are phased with longer duration glacial periods (Jansen et al. 2007), with more limited periods of secondary contact occurring during warmer interglacials of shorter duration. The limited duration for secondary contact implicates secondary contact during the mid-interglacial periods, as temperatures approach their warmest, as opposed to earlier interglacial periods as glacial climatic conditions begin their transition to interglacial conditions.

ISOLATION AND SPECIATION WITH SECONDARY CONTACT IN *A. globulipennis*

Our results suggest that a history of isolation, caused by the fragmentation of suitable habitat, has contributed to the evolution of reproductive isolation between the eastern and western populations of *A. globulipennis*. First, the optimal models from dadi include two rates of migration between eastern and western populations, with approximately 50% of loci experiencing reduced effective migration across the hybrid zone. Limitations to gene flow are also apparent in the clines for allele frequency, admixture, and hybrid index scores. These clines are sharp and geographically coincident with the location of the saddle within the laurel forest. Patterns of hybridization within the contact zone, particularly the presence of individuals of recent hybrid origin inferred from comparison to simulated genotypes, are also consistent with strong reproductive isolation between eastern and western populations (Jiggins and Mallet 2000). Although we do not have any data that directly inform about the nature of selection underlying the barrier to gene flow, the lack of obvious environmental differences either side of the saddle suggests intrinsic incompatibilities are a more important source of reproductive isolation than local adaptation.

BROADER IMPLICATIONS FOR MONTANE CLOUD FOREST BIODIVERSITY

Our results provide support for a Quaternary model of montane cloud forest dynamics that, as far as we are aware, has not been

considered in evolutionary and ecological analyses of montane cloud forest biodiversity. Under the generally accepted model of species ranges being forced upslope by climate warming, and variations within that model (see Ramírez-Barahona and Eguiarte 2013), contemporary lower elevation range limits are inferred to be high relative to interglacial limits. Our results are consistent with both a local climate model by Sperling et al. (2004), and climate model results from the Hawaiian Islands (Lauer et al. 2013) showing that the frequency of TWI conditions increases with warming climate, with the TWI simultaneously occuring at lower elevations. Interpolating this trend to the LGM would mean that montane cloud forests were at higher elevations than the present, as they were not capped by the harsh decrease in humidity that the TWI imposes. The height of the TWI and the frequency of its occurrence can vary from diurnal to millennial time scales (Crausbay et al. 2015). Variations within the Intertropical Convergence Zone, El Niño Southern Oscillation, and Hadley circulation have all been attributed to changes in the height of the TWI (Schubert et al. 1995; Loope and Giambelluca 1998; Sperling et al. 2004; Cao et al. 2007; Crausbay et al. 2015). In oceanic settings, however, a stronger TWI can increase oceanic cloud cover and generally lowers the cloud base height (Stevens 2004; Myers and Norris 2013; Beusekom et al. 2017). This effect could additionally explain downward shifts of cloud forest elevational limits with warming climates in an oceanic setting such as Tenerife.

Our results are, however, in contrast with support for recent upward shifts for cloud base heights inferred from empirical and anecdotal demographic changes in anuran and invertebrate species from Costa Rican cloud forests (Pounds et al. 1999; Janzen and Hallwachs 2019). The reasons for this apparent conflict could be manifold. Cloud base heights over land are generally higher than those over islands, which are closely coupled to the oceanic boundary layer (Beusekom et al. 2017). Upward shifts of both the base height and the frequency of convective and orographic clouds can also be caused by lower elevation deforestation (Lawton et al. 2001; Wang et al. 2009), potentially contributing to observations of upslope shifts of lower range limits of cloud forest species. Another possibility is that our genetic data summarizes a millennial-scale trend, whereas demographic changes in anuran and invertebrate species (e.g., Pounds et al. 1999; Janzen and Hallwachs 2019) capture more recent decadal trends. If variation within a millennial-scale downslope trend of the lower cloud base includes upslope trends over shorter time scales, this could also explain the differences in upward and downward elevational trends between Tenerife and Costa Rica. This gains some support from a 5900-year-long paleorecord of vegetation and fire from 2455 m in the Cordillera Central, Dominican Republic. Upper cloud belt vegetation patterns reveal a downslope shift until approximately 746 AD, after which upslope movement has occurred until the present, explained by coincident shifts in the TWI (Crausbay et al. 2015).

The extent to which the LowCB model describes montane cloud forests from other regions of the globe requires further investigation. We suggest that if it does, it would provide a simple mechanistic explanation for the frequent observation of closely related species that are parapatrically distributed between cloud forest and lower elevations (e.g., Arteaga et al. 2016; Bryja et al. 2018; Eldridge et al. 2018; Gabrielli et al. 2020). Elevational replacement of closely related taxa is both a widely observed phenomenon (e.g., Terborgh 1971; Diamond 1973; Highton 1995; Poynton et al. 2007; Cadena et al. 2012; Jankowski et al. 2013; Dubay and Witt 2014) and an evolutionary paradox, by implying parapatric ecological speciation (Nosil 2012), which is generally accepted to be rare in nature. Under the LowCB model, parapatric speciation across the lower elevation limits of cloud forest does not need to be invoked. Cooler glacial climate conditions would promote allopatry by simultaneously forcing the lower elevation range limits of cloud forest species upslope, and the upper elevation range limits of lower elevation species down slope. Under this model, populations or species that were previously isolated during LGM would now be in secondary contact and hybridizing, and recent genomic data for *Zosterops* on the volcanic island of Reunion are consistent with this model (Gabrielli et al. 2020).

We have demonstrated the power of genomic data to test between competing models of long-term cloud forest response to climate warming. Our results indicate that, over millennial time scales, montane cloud forests in oceanic settings may be subject to downslope shifts of their orographic cloud bases as global temperatures increase, as a consequence of downward shifts of the TWI. However, caution is needed when extrapolating this trend to more continental settings. We concur with Crausbay et al. (2015) that understanding how orographic cloud formations vary over time is fundamental for conservation strategies aimed at protecting tropical mountain ecosystems. To this end, we suggest that understanding local climate change consequences within tropical and subtropical montane cloud forests may benefit from the integration of demographic inference using species that comprise these ecosystems. This is important, as a post-LGM trend for lowering of the TWI, together with recent increases in the elevation of the lower cloud base resulting from local deforestation (Lawton et al. 2001), would imply future contraction of cloud forest ecosystems at both their upper and lower elevational limits.

AUTHOR CONTRIBUTIONS

ASC and BCE designed the study. ASC generated the molecular data with the help of JP. ASC carried out all analyses with input from BCE, SS, and RB. ASC and BCE wrote the manuscript, with all authors contributing to the final version.

ACKNOWLEDGMENTS

This work was financed by the Spanish Agencia Estatal de Investigación (CGL2017-85718-P), awarded to BCE, and co-financed by FEDER. It was also supported by the Spanish Ministerio de Ciencia, Innovación y Universidades (EQC2018-004418-P), awarded to BCE. AS-C was funded by the Spanish Ministerio de Ciencia, Innovación y Universidades through an FPU PhD fellowship (FPU014/02948). The authors thank Instituto Tecnológico y de Energías Renovables (ITER), S.A for providing access to the Teide High-Performance Computing facility (Teide-HPC). Fieldwork was supported by collecting permit AFF 107/17 (sigma number 2017-00572) kindly provided by the Cabildo of Tenerife. The authors wish to thank the following for field work and sample sorting and identification: A. J. Pérez-Delgado, H. López, and C. Andújar. We also thank V. García-Olivares for assistance with laboratory and bioinformatic work.

DATA ARCHIVING

Mitochondrial sequence data and filtered SNP data are available from the Dryad Digital Repository https://doi.org/10.5061/dryad.qz612jmd0. Raw demultiplexed sequences for the full ddRAD-seq data set are available on NCBI SRA BioProject Accession PRJNA668454.

CONFLICT OF INTEREST

The authors declare no conflict of interest.

LITERATURE CITED

Alexander, D. H., J. Novembre, and K. Lange. 2009. Fast model-based estimation of ancestry in unrelated individuals. Genome Res. 19:1655–1664.

Arteaga, A., R. A. Pyron, N. Peñafiel, p. Romero-Barreto, J. Culebras, L. Bustamente, M. H. Yánez-Muñoz, and J. M. Guayasamin. 2016. Comparative phylogeography reveals cryptic diversity and repeated patterns of cladogenesis for amphibians and reptiles in northwestern Ecuador. PLoS One 11:e0151746.

Barton, N. H., and K. S. Gale. 1993. Genetic analysis of hybrid zones. Pp. 13–45 *in* R. G. Harrison, ed. Hybrid zones and the evolutionary process. Oxford Univ. Press, Oxford, U.K.

Beusekom, A. E. V., G. González, and M. A. Scholl. 2017. Analyzing cloud base at local and regional scales to understand tropical montane cloud forest vulnerability to climate change. Atmos. Chem. Phys. 17:7245–7259.

Bolker, B. 2017. bbmle: tools for general maximum likelihood estimation.

Bryja, J., D. Kostin, Y. meheretu, R. Šumbera, A. Bryjová, M. Kasso, O. Mikula, and L. A. Lavrenchenko. 2018. Reticulate Pleistocene evolution of Ethiopian rodent genus along remarkable altitudinal gradient. Mol. Phylogenet. Evol. 118:75–87.

Burnham, K. P., and D. R. Anderson. 2002. Model selection and multimodel inference: a practical information-theoretic approach. Springer-Verlag, New York.

Cadena, C. D., K. H. Kozak, J. P. Gómez, J. L. Parra, C. M. McCain, R. C. K. Bowie, A. C. Carnaval, C. Moritz, C. Rahbek, T. E. Roberts, et al. 2012. Latitude, elevational climatic zonation and speciation in New World vertebrates. Proc. R. Soc. B 279:194–201.

Cao, G., T. W. Giambelluca, D. E. Stevens, and T. A. Schroeder. 2007. Inversion variability in the Hawaiian trade wind regime. J. Clim. 20:1145–1160.

Coffman, A. J., P. H. Hsieh, S. Gravel, and R. N. Gutenkunst. 2016. Computationally efficient composite likelihood statistics for demographic inference. Mol. Biol. Evol. 33:591–593.

Crausbay, S. D., P. H. Martin, and E. F. Kelly. 2015. Tropical montane vegetation dynamics near the upper cloud belt strongly associated with a shifting ITCZ and fire. J. Ecol. 103:891–903.

Cruickshank, T. E., and M. W. Hahn. 2014. Reanalysis suggests that genomic islands of speciation are due to reduced diversity, not reduced gene flow. Mol. Ecol. 23:3133–3157.

Danecek, P., A. Auton, G. Abecasis, C. A. Albers, E. Banks, M. A. DePristo, R. E. Handsaker, G. Lunter, G. T. Marth, S. T. Sherry, et al. 2011. The variant call format and VCFtools. Bioinformatics 27:2156–2158.

Darriba, D., G. L. Taboada, R. Doallo, and D. Posada. 2012. jModelTest 2: more models, new heuristics and parallel computing. Nat. Methods 9:772.

delArco Aguilar, M.-J., W. Wildpret de la Torre, P. L. Pérez de la Paz, O. Rodríguez Delgado, J. R. Acebes Ginovés, A. García Gallo, V. E. Martín Osorio, J. A. Reyes Betencourt, M. Salas Pascual, M. A. Díaz, et al. 2006. Mapa de vegetación de Canarias. GRAFCAN, Santa Cruz de Tenerife, Spain.

Diamond, J. M. 1973. Distributional ecology of New Guinea birds: recent ecological and biogeographical theories can be tested on the bird communities of New Guinea. Science 179:759–769.

Dubay, S. G., and C. C. Witt. 2014. Differential high-altitude adaptation and restricted gene flow across a mid-elevation hybrid zone in Andean tittyrant flycatchers. Mol. Ecol. 2014:3551–3565.

Eaton, D. A. R., and I. Overcast. 2020. ipyrad: interactive assembly and analysis of RADseq datasets. Bioinformatics 36:2592–2594.

Eldridge, R. A., A. S. Achmadi, T. C. Giarla, K. C. Rowe, and J. A. Esselstyn. 2018. Geographic isolation and elevational gradients promote diversification in an endemic shrew on Sulawesi. Mol. Phylogenet. Evol. 118:306–317.

Fjeldså, J., E. Lambin, and B. Mertens. 1999. Correlation between endemism and local ecoclimatic stability documented by comparing Andean bird distributions and remotely sensed land surface data. Ecography 22: 63–78.

Foster, P. 2001. The potential negative impacts of global climate change on tropical montane cloud forests. Earth Sci. Rev. 55:73–106.

Gabrielli, M., B. Nabholz, T. Leroy, B. Milá, and C. Thébaud. 2020. Within-island diversification in a passerine bird. Proc. R. Soc. B 287:20192999.

Guindon, S., and O. Gascuel. 2003. A simple, fast, and accurate algorithm to estimate large phylogenies by maximum likelihood. Syst. Biol. 52:696–704.

Gutenkunst, R. N., R. D. Hernandez, S. H. Williamson, and C. Bustamante. 2009. Inferring the joint demographic history of multiple populations from multidimensional SNP frequency data. PLos Genet. 5:e1000695.

Helmer, E. H., E. A. Gerson, L. S. Baggett, B. J. Bird, S. Ruzycki, and S. M. Voggesser. 2019. Neotropical cloud forests and páramo to contract and dry from declines in cloud immersion and frost. PLoS One 14:e0213155.

Hewitt, G. M. 2000. The genetic legacy of the quaternary ice ages. Nature 405:907–913.

Highton, R. 1995. Speciation in eastern North American salamanders of the genus *Plethodon*. Annu. Rev. Ecol. Syst. 26:579–600.

Huson, D. H., and D. Bryant. 2006. Application of phylogenetic networks in evolutionary studies. Mol. Biol. Evol. 23:254–267.

Jankowski, J. E., G. A. Londoño, S. K. Robinson, and M. A. Chappell. 2013. Exploring the role of physiology and biotic interactions in determining elevational ranges of tropical animals. Ecography 36:001–102.

Jansen, E., J. Overpeck, K. R. Briffa, J.-C. Duplessy, F. Joos, V. Masson-Delmonte, D. Olago, B. Otto-Bliesner, W. R. Peltier, S. Rahmstorf, et al. 2007. Pp. 433–498 Palaeoclimate. *in* S. Solomon, D. Qin, M. Manning, Z. Chen, M. Marquis, K. B. Averyt, M. Tignor, and H. L. Miller, eds. Climate change 2007: the physical science basis. Contribution of work-

ing group i to the fourth assessment report of the intergovernmental panel on climate change, Cambridge Univ. Press, Cambridge, U.K.

Janzen, D. H., and W. Hallwachs. 2019. Perspective: where might be many tropical insects. Biol. Conserv. 223:102–108.

Jiggins, C. D., and J. Mallet. 2000. Bimodal hybrid zones and speciation. Trends Ecol. Evol. 15:250–255.

Keightley, P. D., R. W. Ness, D. L. Halligan, and P. R. Haddrill. 2014. Estimation of the spontaneous mutation rate per nucleotide site in a *Drosophila melanogaster* full-sib family. Genetics 196:313–320.

Keightley, P. D., A. Pinharanda, R. W. Ness, F. Simpson, K. K. Dasmahapatra, J. Mallet, J. W. Davey, and C. D. Jiggins. 2015. Estimation of the spontaneous mutation rate in *Heliconious melpomene*. Mol. Biol. Evol. 32:239–243.

Lauer, A., C. Zhang, and O. Elison-Timm. 2013. Downscaling of climate change in the Hawaii region using CMIP5 results: on the choice of the forcing fields. J. Clim. 26:10006–10030.

Lawton, R. O., U. S. Nair, R. A. Pielke Sr., and R. M. Welch. 2001. Climate impact of tropical lowland deforestation on nearby montane cloud forests. Science 294:584–587.

Loope, L. L., and T. W. Giambelluca. 1998. Vulnerability of island tropical montane cloud forests to climate change, with special reference to East Maui, Hawaii. Clim. Change 39:503–507.

Martin, P. H., T. J. Fahey, and R. E. Sherman. 2010. Vegetation zonation in a Neotropical montane forest: environment, disturbance and ecotones. Biotropica 43:533–543.

Mastretta-Yanes, A., N. Arrigo, N. Alvarez, T. H. Jorgensen, D. Piñero, and B. C. Emerson. 2015. RAD sequencing, genotyping error estimation and de novo assembly optimization for population genetic inference. Mol. Ecol. Resour. 15:28–41.

Matthey-Doret, R., and M. C. Whitlock. 2019. Background selection and Fst: consequences for detecting local adaptation. Mol. Ecol. 28:3902–3914.

Miraldo, A., G. M. Hewitt, P. H. Dear, O. S. Paulo, and B. C. Emerson. 2012. Numts help to reconstruct the demographic history of the ocellated lizard (*Lacerta lepida*) in a secondary contact zone. Mol. Ecol. 21:1005–1018.

Myers, T. A., and J. R. Norris. 2013. Observational evidence that enhanced subsidence reduces subtropical marine boundary layer cloudiness. J. Clim. 26:7507–7524.

Nielsen, E. E., L. Arve Bach, and P. Kotlicki. 2006. HYBRIDLAB (version 1.0): a program for generating simulated hybrids from population samples. Mole. Ecol. Notes 6:971–973.

Nosil, P. 2012. Ecological speciation. Oxford Univ. Press, Oxford, U.K.

Ponce-Reyes, R., V.-H. Reynoso-Rosales, J. E. M. Watson, J. VanDerWal, R. A. Fuller, R. L. Pressey, and H. P. Possingham. 2012. Vulnerability of cloud forest reserves in Mexico to climate change. Nat. Clim. Change 2:448–452.

Pounds, J. A., M. P. L. Fogden, and J. H. Campbell. 1999. Biological response to climate change on a tropical mountain. Nature 398:611–615.

Poynton, J., S. Loader, E. Sherratt, and B. Clarke. 2007. Amphibian diversity in East African biodiversity hotspots: altitudinal and latitudinal patterns. Biodivers. Conserv. 16:1103–1118.

Rahbek, C., M. K. Borregaard, R. K. Colwell, B. Dalsgaard, B. G. Holt, N. Morueta-Holme, D. Nogues-Bravo, R. J. Whittaker, and J. Fjeldså. 2019. Humboldt's enigma: what causes global patterns of mountain biodiversity? Science 365:1108–1113.

Ramírez-Barahona, S., and L. E. Eguiarte. 2013. The role of glacial cycles in promoting genetic diversity in the Neotropics: the case of cloud forests during the Last Glacial Maximum. Ecol. Evol. 3:725–738.

Ronquist, F., M. Teslenko, P. van der Mark, D. L. Ayres, A. Darling, S. Hohna, B. Larget, L. Liu, M. A. Suchard, and J. P. Huelsenbeck. 2012. MrBayes 3.2: efficient bayesian phylogenetic inference and model choice across a large model space. Syst. Biol. 61:539–542.

Rougemont, Q., P.-A. Gagnaire, C. Perrier, C. Genthon, A.-L. Besnard, S. Launey, and G. Evanno. 2017. Inferring the demographic history underlying parallel genomic divergence among pairs of parasitic and nonparasitic lamprey ecotypes. Mol. Ecol. 26:142–162.

Rougeux, C., L. Bernatchez, and P.-A. Gagnaire. 2017. Modeling the multiple facets of speciation-with-gene-flow toward inferring the divergence history of lake whitefish species pairs (*Coregonus clupeaformis*). Genome Biol. Evol. 9:2057–2074.

Salces-Castellano, A., J. Patiño, N. Alvarez, C. Andújar, P. Arribas, J. J. Braojos Ruiz, M.-J. del Arco Aguilar, V. García-Olivares, D. N. Karger, H. López, et al. 2020. Climate drives community-wide divergence within species over a limited spatial scale: evidence from an oceanic island. Ecol. Lett. 23:305–315.

Schubert, W. H., P. E. Ciesielski, C. Lu, and R. H. Johnson. 1995. Dynamical adjustment of the trade wind inversion layer. J. Atmos. Sci. 52:2941–2952.

Sego, L. H. 2016. Smisc: sego miscellaneous. A collection of functions for statistical computing and data manipulation in R. Pacific Northwest National Laboratory. Available via https://pnnl.github.io/Smisc.

Sperling, F. N., R. Washington, and R. J. Whittaker. 2004. Future climate change of the subtropical North Atlantic: implications for the cloud forests of Tenerife. Clim. Change 65:103–123.

Stevens, B. 2004. Atmospheric moist convection. Annu. Rev. Earth Planet. Sci. 33:605–643.

Still, C. J., P. N. Foster, and S. H. Schneider. 1999. Simulating the effects of climate change on tropical montane cloud forests. Nature 398:608–610.

Taylor, S. A., E. L. Larson, and R. G. Harrison. 2015. Hybrid zones: windows on climate change. Trends Ecol. Evol. 30:398–406.

Terborgh, J. 1971. Distribution on environmental gradients: theory and a preliminary interpretation of distributional patterns in the avifauna of the Cordillera Vilcabamba, Peru. Ecology 52:23–40.

Tine, M., H. Kuhl, P.-A. Gagnaire, B. Louro, R. Desmarais, R. S. T. Martins, J. Hecht, F. Knaust, K. Belkhir, S. Klages, et al. 2014. European sea bass genome and its variation provide insights into adaptation to euryhalinity and speciation. Nat. Commun. 5:5770.

van Riemsdijk, I., R. K. Butlin, B. Wielstra, and J. W. Arntzen. 2019. Testing an hypothesis of hybrid zone movement for toads in France. Mol. Ecol. 28:1070–1083.

Wang, J., F. J. F. Chagnon, E. R. Williams, A. K. Betts, N. O. Renno, L. A. T. Machado, G. Bisht, R. Knox, and R. L. Bras. 2009. Impact of deforestation in the Amazon basin on cloud climatology. Proc. Natl. Acad. Sci. USA 106:3670–3674.

Westram, A. M., M. Rafajlović, P. Chaube, R. Faria, T. Larsson, M. Panova, M. Ravinet, A. Blomberg, B. Mehlig, K. Johannesson, et al. 2018. Clines on the seashore: the genomic architecture underlying rapid divergence in the face of gene flow. Evol. Lett. 2–4:297–309.

Associate Editor: D. Filatov
Handling Editor: A. McAdam

Supporting Information

Additional supporting information may be found online in the Supporting Information section at the end of the article.

Figure S1. Bayesian phylogenetic tree of mtDNA COI gene sequences for 253 individuals of *Acalles globulipennis* sampled within the laurel forests of the Anaga peninsula.

Figure S2. Joint distribution of F_{ST} per locus between West and East using individuals of single ancestry (ancestry ≥99.9%), and minor allele frequency (MAF).

Figure S3. Demographic history inference for eastern and western populations of *Acalles globulipennis* using dadi.

Table S1. Sampling sites, Cartesian coordinates, distance from the most western site and altitude.

Table S2. Individual ancestry coefficients for two differentiated genetic clusters (K=2 [West and East]; Salces-Castellano et al. 2019) using ddRAD-seq data.

Table S3. Outputs from dadi analyses and biological estimates for the 11 models analyzed (see Figure 3). Ind = individuals, gen = generations.

Table S4. Parameters of western allele frequency clines: c = center, w = width, Pmax = the maximum observed value for a measure corresponding the western limit of the cline, Pmin = the minimum observed value for a measure corresponding the western limit of the cline.